



Precursory signals of East Asian winter cold anomalies in stratospheric planetary wave pattern

Lei Song¹ · Renguang Wu^{1,2}

Received: 21 June 2018 / Accepted: 7 October 2018 / Published online: 11 October 2018
© Springer-Verlag GmbH Germany, part of Springer Nature 2018

Abstract

The impacts of the stratospheric polar vortex changes on the tropospheric climate variability have been emphasized in previous studies. The present study presents evidence for precursory signals of cold anomalies over East Asia in the stratospheric wave pattern during November through March. The leading two empirical orthogonal function (EOF) modes of daily 50-hPa geopotential height anomalies along 65°N correspond to changes in the amplitude and phase of the stratospheric planetary wavenumber 1, respectively. Composite analysis is performed to unravel the temporal evolution of anomalies during 8 phases of 34 events identified based on the second EOF mode with a complete life cycle for the period 1979–2016. The surface cold anomalies over eastern China emerge in phase 3 (corresponding to negative and positive 50-hPa height anomalies on the North Atlantic and Russian Far East sector, respectively) and peak in phase 5 (corresponding to positive 50-hPa height anomalies over Eurasia) when the Siberian high extends southeastward and the East Asian trough deepens with anomalous surface northerly winds. Downward propagation of stratospheric signal is detected over western Europe and western Siberia. The former is a source region of the tropospheric Rossby wave trains propagating along the polar front jet and subtropical jet. The downward propagation of stratospheric signal is related to the reflection of stratospheric planetary wavenumber 1 pattern and contributes to the development of the tropospheric Rossby wave train that, in turn, leads to the strengthening of the Siberian high and the deepening of the East Asian trough.

Keywords East Asian cold anomalies · Precursory signals · Stratospheric planetary wave pattern · Downward propagation

1 Introduction

There is indication of connections between stratospheric and tropospheric climate variability. On one hand, stratospheric climate may be influenced by the upward propagation of Rossby waves originating from the troposphere (e.g., Charney and Drazin 1961; Scaife and James 2000; Chen et al. 2003). On the other hand, stratospheric climate signals may descend to the troposphere and affect the tropospheric circulations (e.g., Kodera and Kuroda 1990; Baldwin and

Dunkerton 1999; Chen et al. 2005; Scaife et al. 2005; Cai and Ren 2007; Kidston et al. 2015; Yu et al. 2018). Baldwin and Dunkerton (1999) indicated that the Arctic Oscillation (AO) (Thompson and Wallace 1998) anomalies appear first in the stratosphere and then propagate downward and the anomalies reach the surface in a few weeks. They further indicated that the downward propagation of stratospheric AO signal is related to the planetary wave activity.

The impacts of stratospheric variations on surface weather and climate have been shown by previous studies (e.g., Baldwin and Dunkerton 2001; Thompson et al. 2002; Scaife et al. 2005; Kolstad et al. 2010; Tomassini et al. 2012; Woo et al. 2015). The large-scale circulation anomalies in the lower stratosphere can exert a profound influence on the location of the Atlantic and Pacific storm tracks and thus surface weather over the Eurasian continent and North America (Baldwin and Dunkerton 2001; Kidston et al. 2015). The cold air outbreaks over Europe, Asia, and North America are shown to be associated with a weak stratospheric polar vortex (Kolstad et al. 2010). The circulation change during

✉ Renguang Wu
renguang@mail.iap.ac.cn

¹ Center for Monsoon System Research, Institute of Atmospheric Physics, Chinese Academy of Sciences, Beijing, China

² State Key Laboratory of Numerical Modeling for Atmospheric Sciences and Geophysical Fluid Dynamics, Institute of Atmospheric Physics, Chinese Academy of Sciences, Beijing, China

the life cycle of a weak stratospheric polar vortex event influences the temperature variation over East Asia (Woo et al. 2015). Due to the time lag between the stratospheric circulation anomalies and tropospheric cold air outbreaks (e.g., Thompson et al. 2002; Jeong et al. 2006; Scaife et al. 2008), unraveling the precursory stratospheric signals may help the prediction of tropospheric weather and climate.

The impacts of the stratospheric vortex intensity change on tropospheric circulation and climate have been a focus of previous studies (e.g., Kolstad et al. 2010; Mitchell et al. 2013; Woo et al. 2015). In addition to the intensity change, the polar vortex displays changes in its location (Woollings et al. 2010). The displacements of the polar vortex in accompany with the variations of stratospheric planetary wavenumber 1 may play a notable role in tropospheric circulation changes (Mitchell et al. 2013). Therefore, a question of concern in the present study is how winter weather and climate over East Asia is related to the variations in the stratospheric planetary wavenumber 1 pattern.

Many previous studies examined the stratospheric influence on the troposphere in the context of zonal mean changes (Kodera et al. 1990, 2000; Baldwin and Dunkerton 1998, 1999; Wang and Chen 2010; Black 2002; Cai and Ren 2007; Ren and Cai 2007). While these studies have improved greatly the understanding of the troposphere and stratosphere interactions, zonal mean changes cannot capture the regional features of tropospheric circulation changes and weather and climate anomalies (Carlton et al. 2005; Kolstad et al. 2010; Tomassini et al. 2012; Takaya and Nakamura 2013; Kidston et al. 2015; Woo et al. 2015). As the tropospheric response tends to vary with the location and the tropospheric circulation anomalies often display obvious wave patterns, it is necessary to unravel the regional features of tropospheric circulation changes in relation to stratospheric signals. Thus, another issue of concern in the present study is how the stratospheric wave pattern changes influence the regional climate over East Asia.

The reflection of the stratospheric planetary waves is involved in the stratosphere-troposphere coupling (Perlwitz and Harnik 2003; Kodera et al. 2008). Previous studies have indicated that the reflection of the stratospheric planetary waves can modify the tropospheric planetary waves and influence tropospheric weather regimes (Coughlin and Tung 2005; Kodera et al. 2008, 2013, 2016; Nath et al. 2016). Many studies focus on the reflection of stratospheric planetary waves during sudden stratospheric warming (SSW) events. It is worthwhile to identify the reflection of the planetary waves in linking the signals of the stratospheric planetary waves to the occurrence of cold anomalies over East Asia.

Previous studies have identified several regions of the descending of stratospheric signals down to the troposphere in relation to cold events over East Asia. Jeong et al. (2006)

noted that the potential vorticity (PV) anomalies in the stratosphere about 1 week prior to cold surges over East Asia induce rising geopotential height over northern Eurasia. Woo et al. (2015) indicated that the stratospheric height anomalies descend over East Asia and modulate the East Asian trough that in turn affect surface temperature variations. Song et al. (2018) detected intraseasonal height anomalies descending from the stratosphere over west Europe. A question is where the preferred regions are for the stratospheric signals to descend to the troposphere prior to cold anomalies over East Asia. This question is related to the issue about the regional features of the tropospheric circulation changes in relation to the stratospheric signal.

The present study focuses on the impacts of stratospheric planetary wave changes on the occurrence of East Asian cold anomalies in boreal winter. The rest sections are organized as follows. The dataset and methodology are described in Sect. 2. In Sect. 3, the features of the stratospheric planetary wave pattern in the high latitudes are discussed by empirical orthogonal function (EOF) analysis and lead-lag regression. The East Asian climate anomalies associated with the stratospheric planetary wave pattern are presented in Sect. 4. The specific regions for stratospheric signals to affect tropospheric circulations are analyzed in Sect. 5. A summary of results and some discussions are provided in Sect. 6.

2 Data and methodology

The present study uses daily variables from the National Centers for Environmental Prediction (NCEP)–Department of Energy (DOE) Reanalysis 2, which is provided by the National Oceanic and Atmospheric Administration/Office of Oceanic and Atmospheric Research/Earth System Research Laboratory (NOAA/OAR/ESRL) Physical Science Department (PSD) (Kanamitsu et al. 2002). The variables include surface air temperature, surface wind, sea level pressure, geopotential height, meridional wind, and zonal wind at different pressure levels. The pressure level variables have a horizontal resolution of $2.5^\circ \times 2.5^\circ$ with 17 levels extending from 1000- to 10-hPa. The surface variables are on the T62 Gaussian grid. The NCEP-DOE reanalysis data cover the period from January 1979 to the present.

In order to identify the variations of high latitude stratospheric planetary waves, we apply the EOF analysis to the correlation matrix of daily geopotential height anomalies along 65°N at 50-hPa from November to March of the year 1979–2016. The reason we choose the time span of November to March is that it is active season for the stratosphere-troposphere interaction in the North Hemisphere (Baldwin et al. 2003; Black and McDaniel 2007; Woollings et al. 2010). Because the maximum amplitude of wavenumber 1 pattern is situated around 65°N in the stratosphere (Wang

et al. 2009), we use the geopotential height field along 65°N to perform the EOF analysis. Composite analysis is employed to examine the evolution of anomalies during the life cycle of the wavenumber 1 pattern in Sect. 4. The significance of composite anomalies is estimated by the Student's *t* test. The intensity of the Siberian high is represented using the mean sea level pressure averaged over the region of 40°N–65°N and 80°E–120°E (Panagiotopoulos et al. 2005).

In this study, we use the Rossby wave activity flux (Takaya and Nakamura 1997, 2001) to illustrate the horizontal and vertical propagation of tropospheric Rossby wave. The three-dimensional wave activity flux writes:

$$W = \frac{P_0}{2|\vec{V}|} \left\{ \begin{array}{l} \bar{u}(v'^2 - \psi'v'_x) + \bar{v}(-u'v' + \psi'u'_x) \\ \bar{u}(-u'v' + \psi'u'_x) + \bar{v}(u'^2 + \psi'u'_y) \\ \frac{f_0 R}{N^2 H_0} [\bar{u}(v'T' - \psi'T'_x) + \bar{v}(-u'T' - \psi'T'_y)] \end{array} \right\}$$

The propagation of planetary wavenumber 1 is depicted by the Eliassen-Palm (EP flux) (Andrews et al. 1987) and Plumb flux (Plumb 1985). The Fourier harmonics is used to extract planetary wavenumber 1 pattern (Chen et al. 2005).

3 The stratospheric planetary wavenumber 1 variation

The present study aims at investigating the influence of the stratospheric planetary wave patterns on the tropospheric climate. For this purpose, we first analyze the features of dominant modes of stratospheric planetary waves. The stratospheric planetary wave patterns are modulated by both wavenumber 1 and 2 modes (Woollings et al. 2010). In comparison, the wavenumber 2 modes account for less percent variance compared to the wavenumber 1 modes (Woollings et al. 2010). We focus on the influence of the wavenumber 1 modes.

Figure 1a presents the spatial distribution of the leading two EOF modes of daily geopotential height anomalies along 65°N at 50-hPa during November–March for the period 1979–2016. The first and second modes account for 31.6 and 22.4% of the total variance, respectively. They can be separated from the other modes according to the criterion of North et al. (1982). The centers of positive and negative geopotential height anomalies of EOF1 are located around 110°W and 50°E, respectively. The centers of positive and negative geopotential height anomalies of EOF2 are near 170°E and 20°W, respectively. A similar EOF analysis is performed along 55°N. The obtained leading two modes display spatial patterns similar to those along 65°N with the large loading regions located eastward.

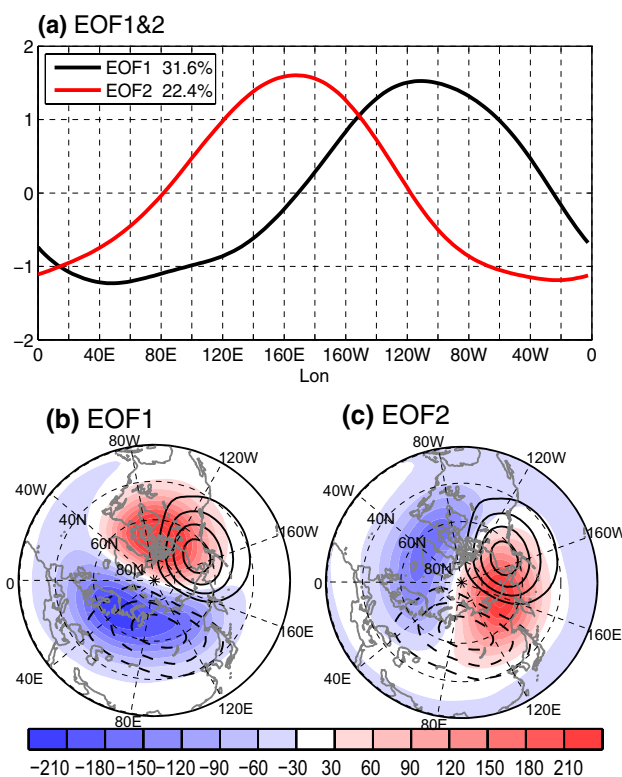


Fig. 1 EOF1 and EOF2 (a) of daily geopotential height anomalies (gpm) at 50-hPa along 65°N for NDJFM. The numbers at top-left denote the percent variances accounted for by EOF1 and EOF2. Geopotential height anomalies at 50-hPa (shading) obtained by regression onto normalized PC1 (b) and PC2 (c) superposed with the deviation of climatology mean geopotential height at 50-hPa from its zonal mean for NDJFM (contour with interval of 80 gpm)

The two modes have a different modulation of the stratosphere planetary wave. This is demonstrated in Fig. 1b–c that compare the stationary wave distribution and the EOF modes-related geopotential height anomalies at 50-hPa. The stationary wave is obtained as the departure of climatological mean from its zonal mean. The geopotential height anomalies corresponding to the two modes are obtained by regression onto the normalized principal component (PC1 and PC2) time series. The climatological mean departure is manifested as roughly wavenumber 1 pattern, with positive center located around Alaska and negative center situated around western Siberia, respectively (Fig. 1b, c). The EOF1 pattern displays an overlap with the stationary wave. This indicates that the EOF1 mode modulates largely the amplitude of the stationary wave. The EOF1 pattern in our study is similar to the EOF2 pattern obtained by Woollings et al. (2010). In contrast, the EOF2 pattern tends to be orthogonal with respect to the stationary wave pattern. This suggests that the EOF2 mode may induce displacement of the stationary wave.

The lead-lag relationship between PC1 and PC2 varies from year to year. A significant positive correlation is detected when PC2 leads PC1 by about two weeks in 23 of the 37 years (figure not shown). In the other 14 years, the correlation coefficient is negative when PC2 leads PC1 by 3–24 days. Here, we show the lead-lag regression maps of geopotential height anomalies with respect to normalized PC1 (Fig. 2a) and PC2 (Fig. 2b) based on these 23 years. There are negative height anomalies over the polar region on –25 days, indicative of a strong polar vortex. The negative anomalies move towards the North Atlantic Ocean, meanwhile, positive anomalies emerge over northeastern Eurasia, forming a dipole distribution similar to the PC2 pattern (–20 day and –15 day). The positive anomalies over Eurasia then weaken and move westward and new positive anomalies appear over North America (–10 day). From –5 day, the distribution becomes similar to the PC1 pattern and the magnitude increases (Fig. 1b). After +5 day, the dipole pattern weakens (+5 to +15 day). On

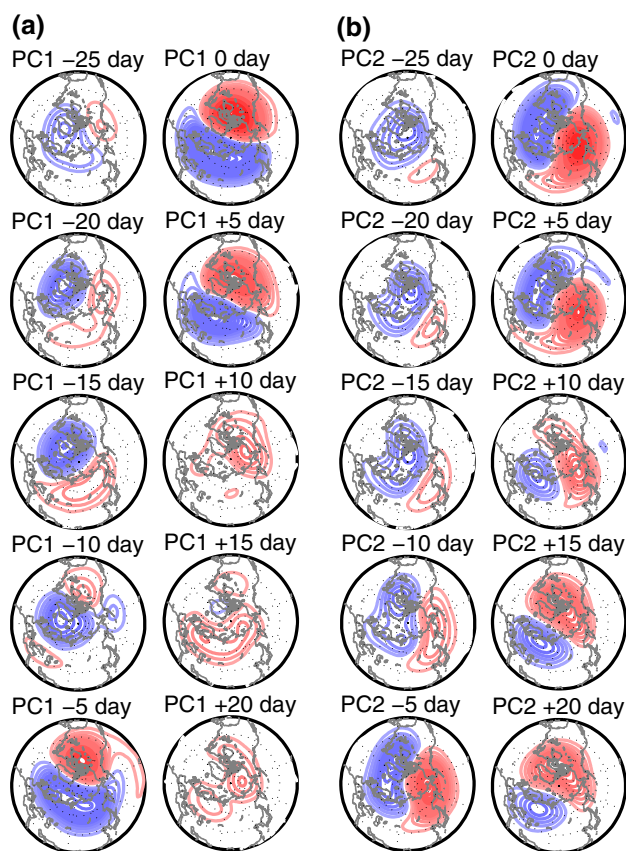
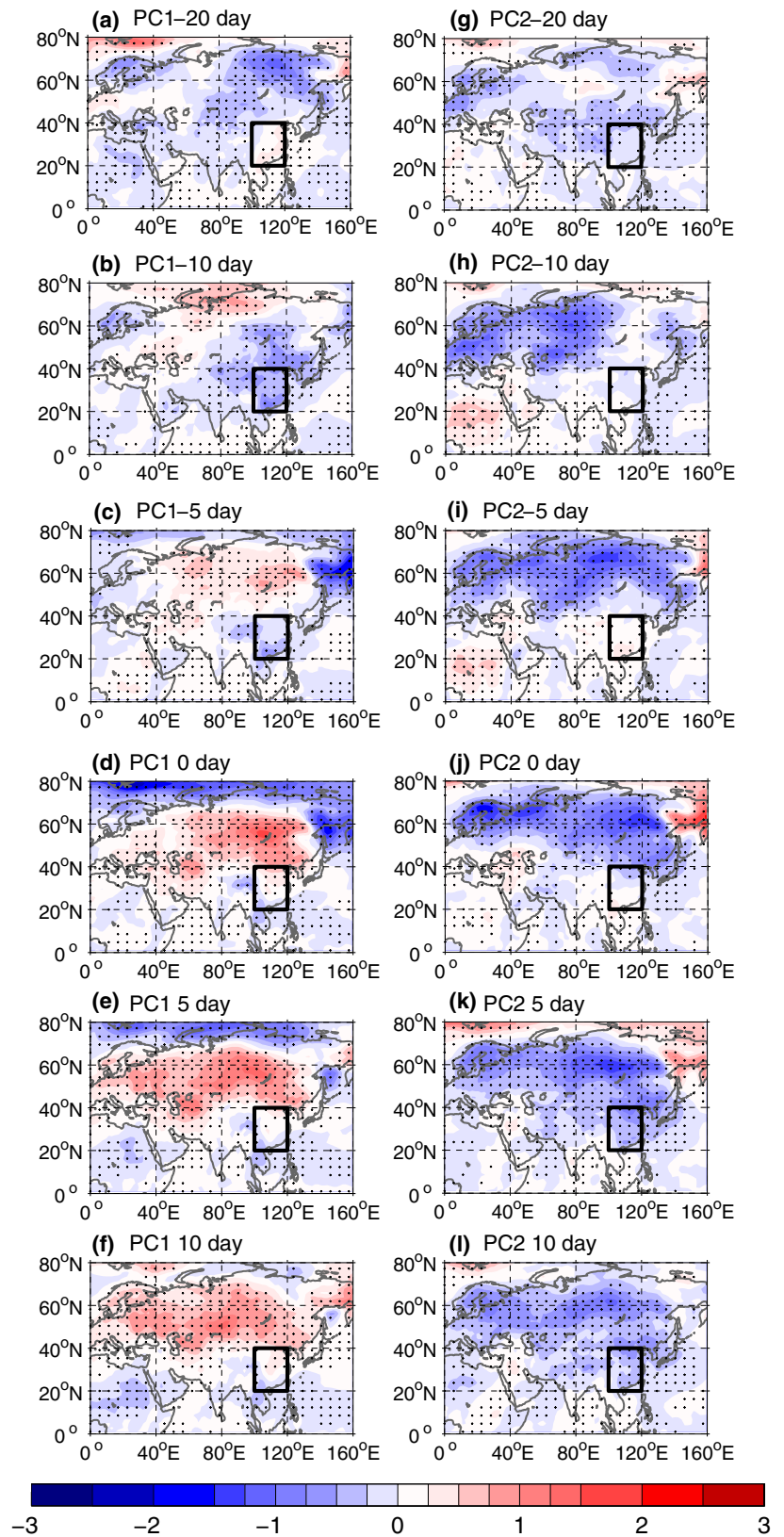


Fig. 2 Geopotential height anomalies (gpm) at 50-hPa in NDJFM obtained by regression unto normalized PC1 (a) and PC2 (b) based on 23 years in which PC1 lags PC2 by about 15–20 days. Negative (positive) days denote height anomalies leading (lagging) PC1 or PC2. The negative values are in blue contour, and positive values are in red contour. The contour interval is 10 gpm. The region shown is the Northern Hemisphere north of 20°N with Eurasia on the bottom

lead-lag regression maps of geopotential height anomalies with respect to PC2 (Fig. 2b), negative height anomalies occupy the polar region from –25 day to –15 day. Meanwhile, positive anomalies increase over eastern Eurasia. The distribution becomes similar to the PC2 pattern from –10 day (Fig. 2a). After +5 day, the anomalies weaken and move eastward and the distribution becomes the PC1 pattern (Fig. 1b) on +15 day. This indicates that the PC2 leads PC1 by about 15 to 20 days.

Previous studies have indicated the influence of the stratospheric polar vortex strength upon the tropospheric climate (Kolstad et al. 2010; Tomassini et al. 2012; Takaya and Nakamura 2013; Kidston et al. 2015; Woo et al. 2015). Here, we show that the East Asian winter climate anomalies have a good relationship to the stratospheric planetary wavenumber 1 patterns. This is demonstrated in Fig. 3 that displays the lead-lag regression of surface air temperature anomalies with respect to normalized PC1 and PC2 time series. Negative temperature anomalies appear west and north of the Lake Baikal when temperature anomalies lead PC1 by 20 days (Fig. 3a). The temperature anomalies move southeastward afterwards. The negative temperature anomalies are situated over eastern China when leading PC1 by 10 days (Fig. 3b). Then, the cold anomalies diminish and warm anomalies emerge around the Lake Baikal (Fig. 3c). The warm anomalies are confined to north of 40°N with a large zonal extension, so the temperature anomalies are weak over eastern China since PC1 starts to lead temperature anomalies (Fig. 3d–f). Weak cold anomalies are observed south of the Lake Baikal when temperature anomalies lead PC2 by 20 days (Fig. 3g). These temperature anomalies are diminished afterwards. Negative temperature anomalies appear over Europe and western Siberia when temperature anomalies lead PC2 by 10 days (Fig. 3h). Then, the cold anomalies extend eastward (Fig. 3i–j) and intrude eastern China when PC2 lead temperature anomalies by 5–10 days (Fig. 3k, l). The evolution of temperature anomalies averaged over eastern China (20°N–40°N, 100°E–120°E) with respect to normalized PC1 and PC2 time series is presented in Fig. 4. Negative temperature anomalies are observed about 10 days before the peak PC1 and about 6 days after the peak PC2. This time difference is consistent with the lead-lag relationship between PC1 and PC2. This indicates a significant influence of stratospheric planetary wavenumber 1 modes on the occurrence of cold anomalies over East Asia, especially over eastern China. The temperature anomalies over eastern China with respect to PC1 are weaker than those with respect to PC2 when the time lag is shorter than 10 days. This indicates a closer relationship between the variations of PC2 and temperature over eastern China. So, we focus on the variation of PC2 and its influence on climate anomalies over eastern China. The influence of the

Fig. 3 Surface temperature anomalies ($^{\circ}\text{C}$, shading) in NDJFM obtained by regression onto normalized PC1 (a) and PC2 (b) based on 23 years in which PC1 lags PC2 by about 15–20 days. Negative (positive) days denote temperature anomalies leading (lagging) PC1 or PC2. Black dots indicate anomalies significant at the 95% confidence level. Black boxes denote the regions where area-mean temperature anomalies are calculated in Fig. 4



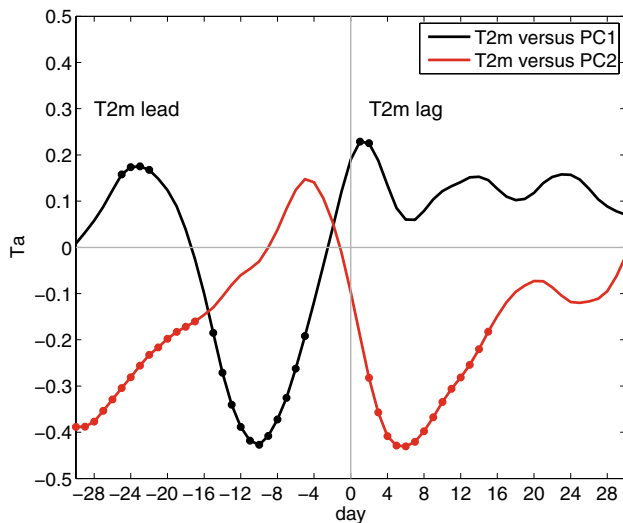


Fig. 4 Surface air temperature anomalies ($^{\circ}\text{C}$) in NDJFM averaged in the region of 20°N – 40°N and 100°E – 120°E obtained by regression on normalized PC1 (black curve) and PC2 (red curve) based on 23 years in which PC1 lags PC2 by about 15–20 days. Negative (positive) day denotes temperature leading (lagging) PC1 or PC2. Marked points indicate anomalies significant at the 95% confidence level

PC1 variation may be inferred according to the time lag relationship between PC1 and PC2.

4 The stratospheric planetary wave pattern-related East Asian climate anomalies

The previous section provides evidence for a connection of the cold anomaly over eastern China with the stratospheric planetary wave pattern. In this section, we examine the temporal evolution of stratospheric and tropospheric

anomalies during the life cycle of PC2 to understand the physical linkage. For this purpose, we first classify the temporal evolution of PC2 into 8 phases based on identified typical events during November–March of 1979–2016. Then, we perform a composite analysis of anomalies in these events.

The typical events with a complete life cycle are identified based on the evolution and amplitude of normalized PC2 time series. A typical event consists of a temporal evolution starting from 0, growing to the peak, then decreasing to negative, reaching the negative lowest, and turning back to 0. The whole life cycle for a typical event is divided into eight phases: phase 1 is the day when PC2 is close to 0 in the transition from negative to positive value, phase 3 is the day when PC2 reaches the largest positive value with the magnitude exceeding one standard deviation, phase 5 is the day when PC2 is close to 0 during the transition from positive to negative value, and phase 7 is the day when PC2 reaches the lowest negative value with the magnitude exceeding one standard deviation. Phase 2 is defined as the day located just in the middle of phase 1 and phase 3. Similarly, phase 4 is the day located in the middle day between phase 3 and phase 5, and phase 6 is the day in the middle of phase 5 and phase 7. If PC2 recovers to 0 after phase 7, the day in the middle of phase 7 and the day with PC2 near 0 is defined as phase 8. We detect 34 events with a complete life cycle in the study period (1979–2016). The days of phase 3 and phase 7 are shown in Table 1. The longest time interval between phase 3 and phase 7 is 52 days (2001–2002), and the shortest time interval is 8 days (1980–1981). The mean time interval between phase 3 and phase 7 is 17 days. So, the mean time interval from one phase to its next phase is about 4 days on average. One thing to note is that composite anomalies obtained based on the PC2 phases of selected events are not directly comparable to those obtained by the

Table 1 The years and the days of phase 3 and phase 7 of PC2 life cycle

Year	Phase 3 and phase 7 day	Year	Phase 3 and phase 7 days
1980–1981	Feb 8, Feb 16	1996–1997	Jan 20, Feb 6; Feb 25, Mar 9
1981–1982	Nov 26, Dec 7; Feb 8, Feb 18	1998–1999	Jan 9, Jan 30
1983–1984	Jan 19, Jan 29	1999–2000	Nov 27, Dec 8; Dec 27, Jan 15
1984–1985	Feb 15, Mar 3	2001–2002	Dec 2, Dec 24; Dec 31, Feb 21
1985–1986	Dec 28, Jan 20; Feb 21, Mar 15	2004–2005	Nov 19, Dec 7; Jan 7, Jan 15
1988–1989	Feb 6, Mar 6	2007–2008	Dec 4, Dec 25
1989–1990	Dec 11, Dec 30; Jan 19, Feb 8	2009–2010	Feb 4, Mar 3
1990–1991	Jan 7, Jan 16	2010–2011	Dec 1, Dec 15; Dec 25, Jan 4
1991–1992	Dec 5, Dec 19	2012–2013	Dec 6, Jan 18; Jan 27, Feb 13
1992–1993	Jan 15, Feb 1; Feb 19, Mar 9	2014–2015	Jan 10, Jan 28
1993–1994	Dec 13, Dec 28; Feb 24, Mar 4	2015–2016	Jan 14, Jan 24
1994–1995	Feb 13, Feb 21		

See the text for definition of the events

lead-lag regression of the geopotential height anomalies with respect to PC2 (Fig. 2) as the time interval between neighboring phases varies largely among different PC2 cycles.

During phase 1, negative geopotential height anomalies at 50-hPa extend from Siberia through the Arctic to Greenland with the center located over central Siberia (Fig. 5a). Positive height anomalies cover the North Pacific and Alaska. Another region of positive height anomalies sits over Northern Europe. The negative anomalies move westward and equatorward from phase 1 to phase 3 with an increase in the magnitude (Fig. 5a–c). At the same time, the positive anomalies over the North Pacific in phase 1 move westward and intensify. The distribution of geopotential height anomalies in phase 3 is identical to that in the instantaneous regression maps of PC2 (Figs. 1c, 2b). From phase 3 to phase 5, the negative anomalies move clockwise and weaken slightly and the positive anomalies also move clockwise with somewhat decrease in the magnitude (Fig. 5c–e). In phase 5, the negative anomalies are located over North America and the Arctic Ocean and the positive anomalies cover Eurasia (Fig. 5e). From phase 5 to phase 7, the dipole continues to move clockwise and the anomalies increase (Fig. 5e–g). The location of the dipole in phase 7 is close to that in phase 3 except with opposite signs (Fig. 5c, g). In phase 8, the anomalies weaken somewhat (Fig. 5h).

Previous studies have indicated that both the displacement and the split types of the SSW events are related to

the variation of the planetary wavenumber 1 (Bancalá et al. 2012; Mitchell et al. 2013; Barriopedro and Calvo 2014; Kodera et al. 2016). The reversal of the 10-hPa westerly at 60°N is used to define the SSW event (Kodera et al. 2016). We have examined the evolution of westerly winds at 10-hPa along 60°N (figure not shown). Reversal of the westerly winds during the eight phases of the PC2 life cycle is not observed. The signals of the SSW events may be reduced largely by the composite analysis.

During phase 1 and phase 2, eastern China is covered by moderate positive temperature anomalies (Fig. 6a, b). The cold anomalies appear over this region in phase 3, but the main body of the cold anomalies is located north of 40°N around the Lake Baikal at this time (Fig. 6c). The cold anomalies begin to move southward after phase 3. In phase 4, the negative temperature anomalies reach 20°N (Fig. 6d). After that, the negative temperature anomalies south of 40°N strengthens, whereas those north of 40°N are weakened (Fig. 6e). This temperature anomaly pattern is similar to that in the strong cold events of eastern China south of 40°N addressed by Song and Wu (2017). After phase 5, the cold anomalies diminish (Fig. 6f–h).

The cold events over East Asia often occur when the Siberian high intensifies and strong northerly surface winds blow (Ding and Krishnamurti 1987; Zhang et al. 1997; Jeong and Ho 2005; Song and Wu 2017). The cold anomalies over southern China are closely related to the advection of mean temperature by anomalous surface meridional winds (Song

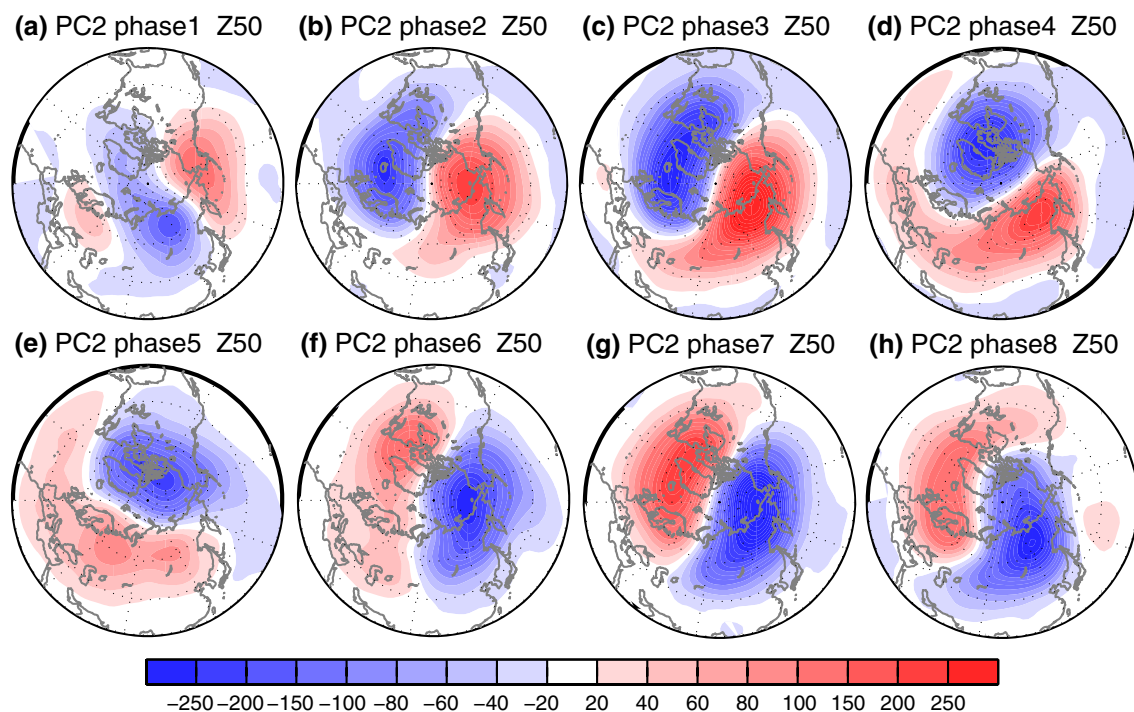
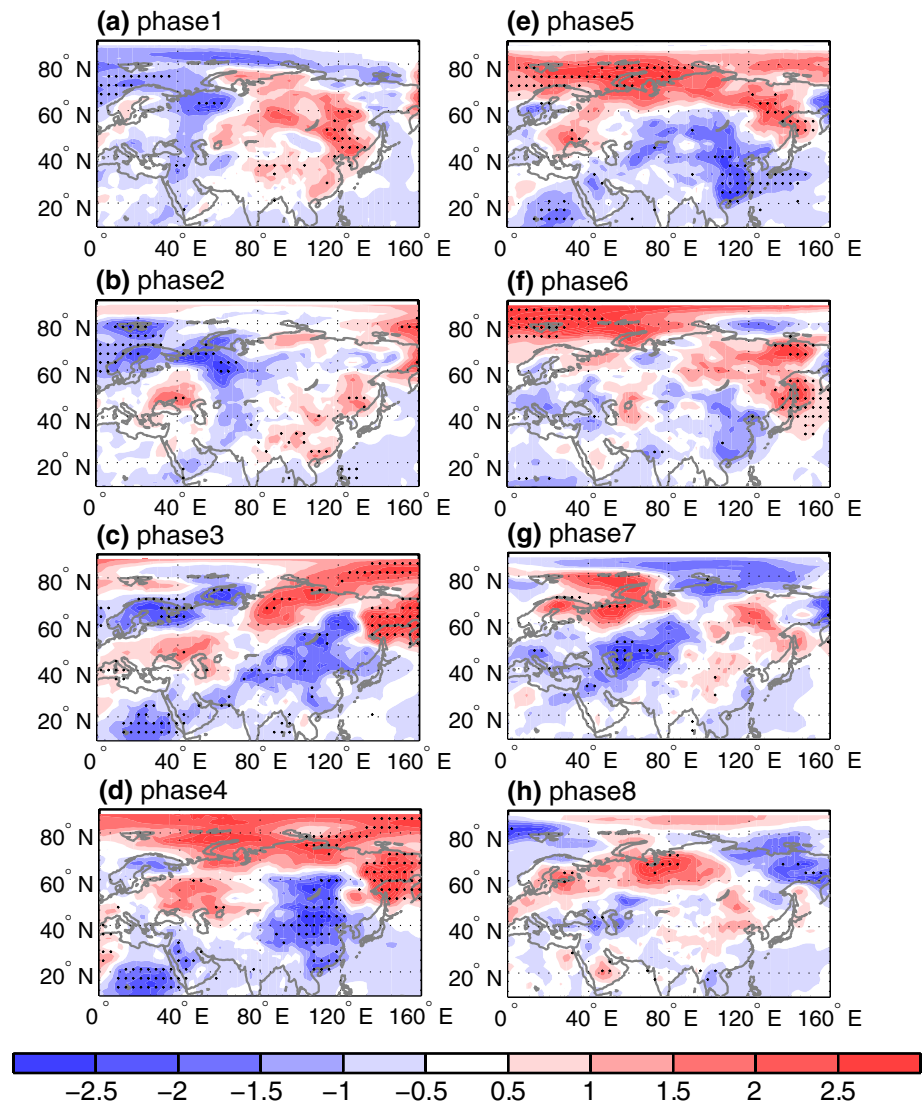


Fig. 5 Composite geopotential height anomalies (gpm) at 50-hPa in phases 1–8 of PC2 life cycle

Fig. 6 Composite surface air temperature anomalies ($^{\circ}\text{C}$) in phases 1–8 of PC2 life cycle. The black dots indicate anomalies significant at the 95% confidence level

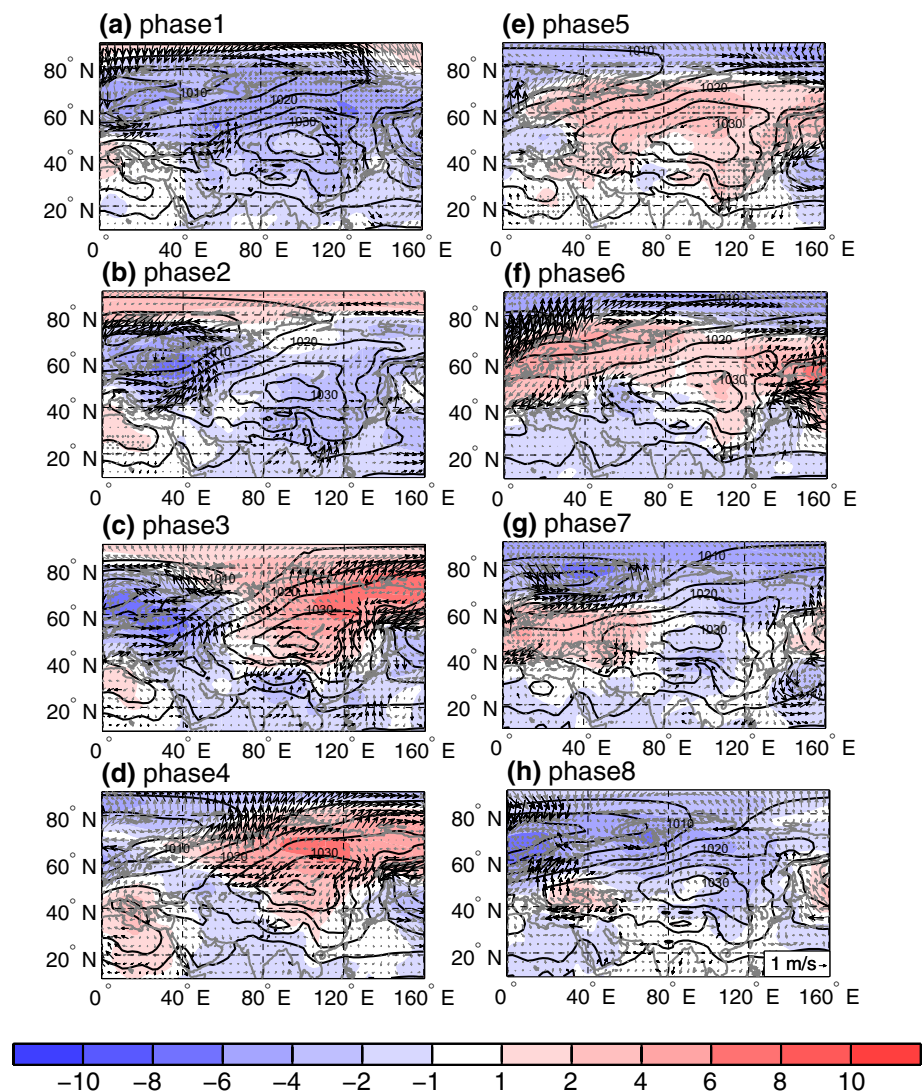


and Wu 2017). In phase 1 and phase 2, the surface wind and sea level pressure anomalies over eastern China are weak (Fig. 7a, b). In phase 3, the Siberian region is covered by a strong anomalous anticyclone (Fig. 7c). This indicates the strengthening of the Siberian high and the associated development of anomalous lower-level northerly winds over the southeastern flank of the anticyclone. These anomalous winds bring colder air from higher latitudes, leading to the accumulation of cold air around the Lake Baikal (Fig. 6c). After phase 3, the anomalous anticyclone extends southward, indicating the southeastward extension of the Siberian high (Fig. 7d, e). The anomalous northerly winds over East Asia reach south of 40°N (Fig. 7d, e), accompanied by the southward intrusion of cold air to eastern China (Fig. 6d, e). In phase 5, the south flank of the anticyclone is near 20°N , suggesting a significant southeastward extension of the Siberian high (Fig. 7e). After phase 5, the anticyclone retreats, and the surface northerly winds weaken (Fig. 7f–h).

Meanwhile, the surface temperature anomalies become weak (Fig. 6g, h).

The happening of cold events over East Asia is related to the deepening of the East Asian trough and a mid-tropospheric wave pattern over Eurasia along the polar front jet (Song et al. 2016, 2018). In phase 3 and phase 4, a Rossby wave train is observed over the mid-high latitude Eurasia (Fig. 8c, d) with negative height anomalies over Europe (0°E – 40°E and 50°N – 70°N), positive height anomalies over western Siberia (80°E – 120°E , 50°N – 70°N), and negative height anomalies over East Asia (80°E – 120°E , 20°N – 40°N). There is a westward extension of the positive geopotential height anomalies along 65°N from 80°E to 40°E , which may contribute to the establishment of the wave train (Fig. 8c). This westward extension of tropospheric height anomalies corresponds to the clockwise movement of the positive geopotential height anomalies at 50-hPa in phases 2–3 (Fig. 5b, c). This correspondence indicates a possible influence of

Fig. 7 Same as Fig. 6, but for surface wind anomalies (vector; scale on right-bottom of phase 8), sea level pressure (hPa) (contour), and sea level pressure anomalies (shading). The gray dots and black vectors indicate anomalies significant at the 95% confidence level. The contour interval is 5 hPa



the stratospheric circulation on the development of tropospheric anomalies. Song et al. (2018) has revealed that the intraseasonal Rossby wave train over the mid-high latitude Eurasian continent associated with cold events over eastern China is triggered by the downward propagation of stratospheric anomalies over western Europe. We will discuss the stratospheric trigger of the tropospheric Rossby wave train during the PC2 life cycle in the next section. The negative geopotential height anomalies over East Asia are intensified in phase 4, accompanying the southwestward extension of the positive height anomalies over western Siberia (Fig. 8d). The northwesterly winds lead to the accumulation of cold air around the Lake Baikal (Fig. 6c, d), which favors the intensification of the Siberia high (Fig. 7c, d). At the same time, the East Asian trough deepens and extends southwestward from the Sea of Okhotsk to northeast China around the longitude of 130°E (Fig. 8d), which favors the southeastward expansion of the Siberian high and the development of anomalous

northerly surface winds along with the advection of cold air from higher latitudes to south of 40°N (Fig. 7d). After phase 4, the wave train displaces westward and the East Asian trough weakens (Fig. 8e, f). In phases 7–8, a wave train with opposite anomalies develops over the mid-high latitude Eurasia (Fig. 8g, h), which is followed by a weakening of the East Asian trough and an anomalous surface low over East Asia (Fig. 7h). These correspond to the reversal of geopotential height anomalies at 50-hPa (Fig. 5g, h).

The relations among the stratospheric wave pattern, tropospheric circulation, and eastern China surface temperature variations are further illustrated in Fig. 9 that are composite anomalies in the eight phases of PC2 life cycle. The surface temperature anomalies over eastern China are the average over the domain of 20°N–40°N and 100°E–120°E. The geopotential height anomalies at 500-hPa are the average over the same region, which are used to denote roughly the strength of the East Asian trough.

Fig. 8 Composite geopotential height (gpm) (contour) and geopotential height anomalies (gpm) (shading) at 500-hPa in phases 1–8 of PC2 life cycle. The black dots in the figures indicate anomalies significant the 95% confidence level. The contour level is 100 gpm

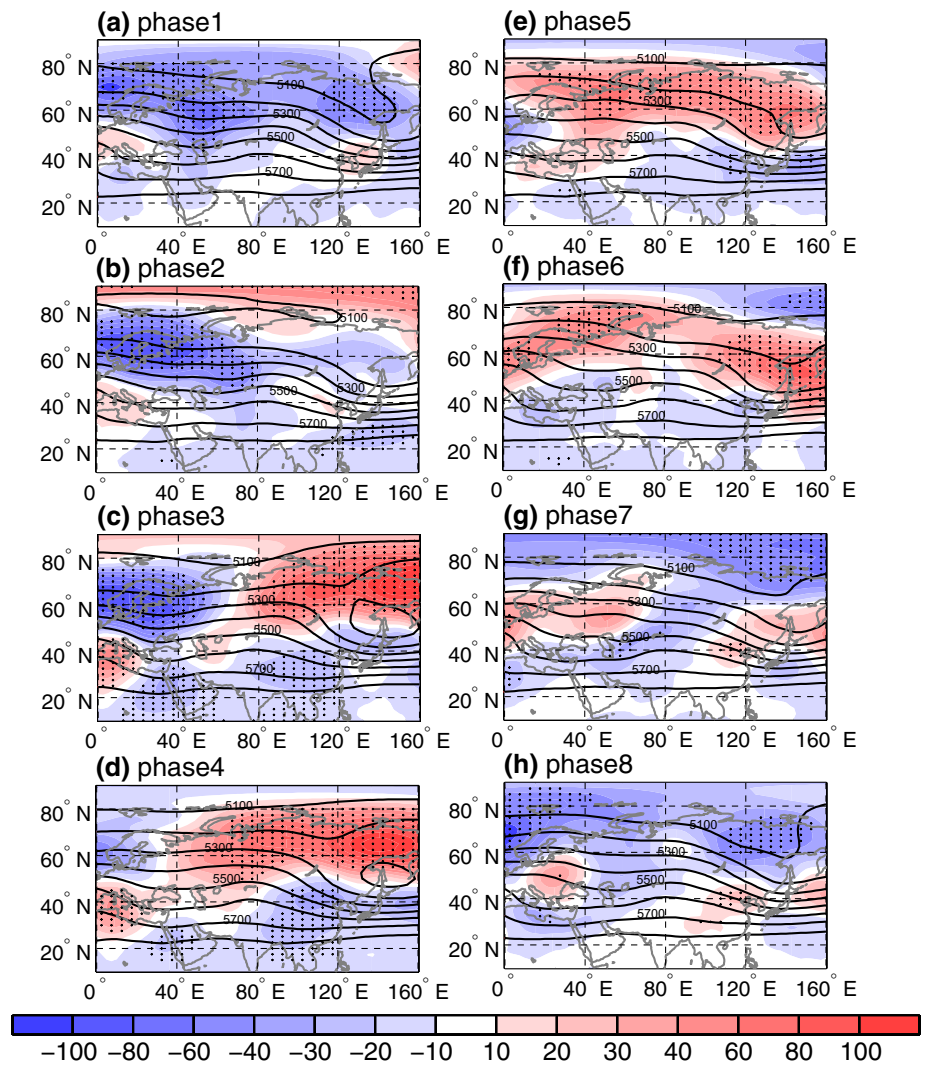
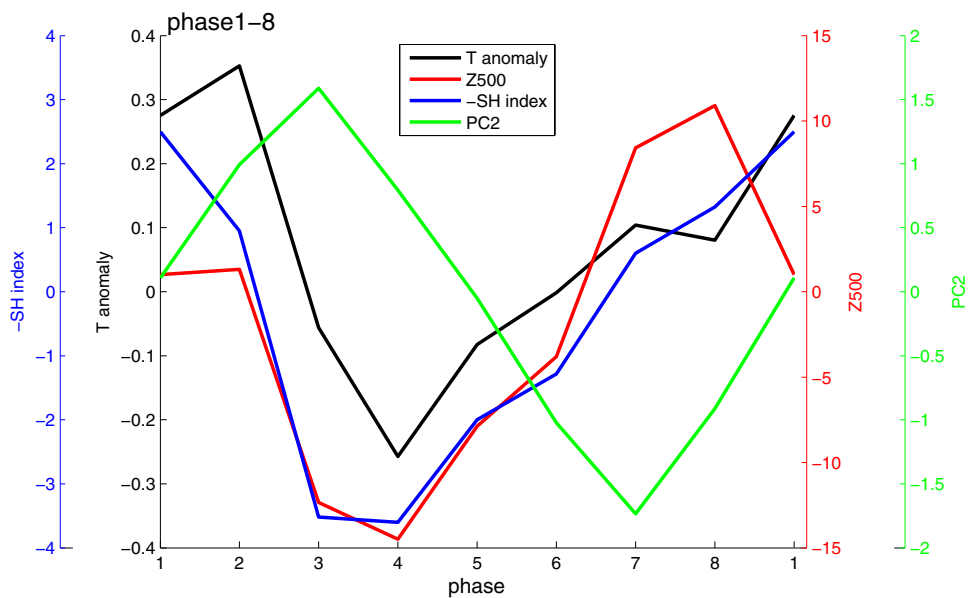


Fig. 9 Time evolution of regional mean surface air temperature anomalies ($^{\circ}\text{C}$) and geopotential height anomalies (gpm) in the region of 20°N – 40°N and 100°E – 120°E , the Siberian high index (hPa), and normalized PC2 in phases 1–8 of PC2 life cycle



The Siberian high index is defined using sea level pressure anomalies averaged over the region of 40°N–65°N and 80°E–120°E, following Panagiotopoulos et al. (2005). The surface temperature drops from phase 2 to phase 4, following the intensification of the Siberian high and the East Asian trough. The time lag supports the effect of the intensification of the East Asian trough and the intensification and southward expansion of the Siberian high on the occurrence of cold anomalies in eastern China (Panagiotopoulos et al. 2005; Takaya and Nakamura 2013; Song and Wu 2017). The Siberian high index evolves in the same pace as the geopotential height anomalies at 500-hPa, suggesting a close relationship between the intensification of the Siberian high and the East Asian trough development (Song et al. 2016). The tropospheric circulation anomalies lag the stratospheric planetary wave pattern, indicative of the precursory stratospheric signal. Note that the decrease of PC2 lags the decrease of the other 3 indices by 1 phase, and the increase of PC2 lags the increase of the other 3 indices by 3 phases. This phase relation suggests that the

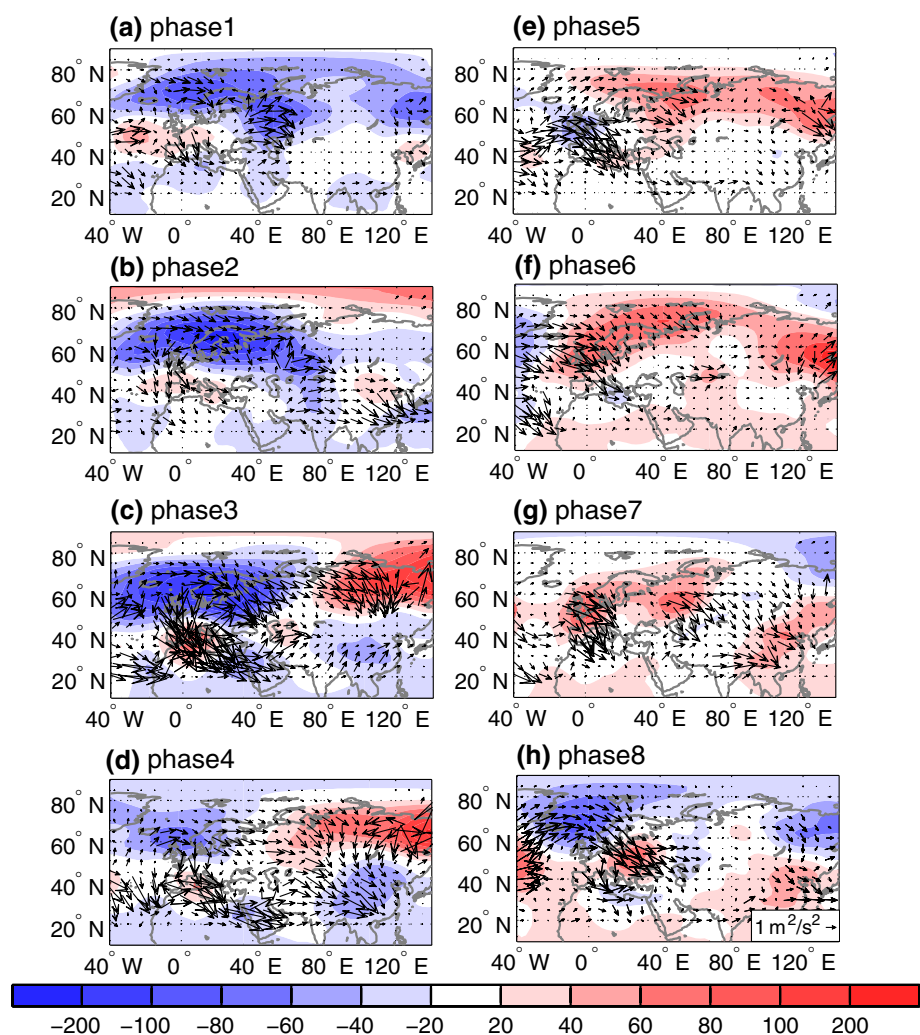
tropospheric anomalies may influence the stratospheric planetary waves, which is beyond the scope of the present study.

5 The stratospheric planetary wave pattern-induced tropospheric anomalies

Previous section provides evidence of stratospheric signal in tropospheric circulation changes. In this section, we investigate possible physical connection between the variation of the stratospheric wave pattern and tropospheric circulation anomalies. For this purpose, we first analyze the tropospheric wave propagation to identify the source regions. Then, we explore whether the tropospheric changes in the wave source regions are subjected to stratospheric influences.

The propagation of tropospheric Rossby wave packet is illustrated by the Rossby wave activity fluxes at 300-hPa (Takaya and Nakamura 1997, 2001). The wave pattern in

Fig. 10 Same as in Fig. 8, but for geopotential height anomalies at 300-hPa (gpm) (shading) and wave activity flux (unit m^2/s^2) (vector, scale on right-bottom of the last panel)



geopotential height anomaly field over mid-high latitude Eurasia is weak in phases 1–2 and becomes evident in phases 3–4 (Fig. 10a–d). The wave activity fluxes appear to be emitted from the source over northwestern Europe in phase 3 (Fig. 10c). This region corresponds to that where intraseasonal Rossby wave train is triggered by stratospheric anomalies (Song et al. 2018). The wave fluxes split into two branches, one propagating along the polar front jet and the other propagating southward to the Mediterranean Sea (Fig. 10c, d). The Mediterranean Sea may act as a wave source (Watanabe 2004) from where the wave packet propagates along the subtropical waveguide towards East Asia. This subtropical wave is detected in strong cold events which are confined to north of 40°N by Song and Wu (2017). The two branches of wave packets propagate toward East Asia (Fig. 10d), contributing to the East Asian trough change. The establishment of the north wave train may be contributed by the westward extension of the positive height anomalies from northeast Eurasia (Fig. 10c, d). After phase 4, the wave trains over the Eurasian continent are weakened (Fig. 10e–h).

In the following, we examine the possible downward propagation of stratospheric signals in several key regions. The first region is the northwestern Europe that appears to be a source region of the tropospheric Rossby wave train (Fig. 10c). Song et al. (2018) identified downward propagation of intraseasonal signal from the stratosphere in this region. The second region is western Siberia where tropospheric height anomalies increase from phase 3 to 4, following an increase of same-sign height anomalies in the stratosphere (Fig. 10c, d). The third region is East Asia where negative height anomalies at 300-hPa develop and positive sea level pressure anomalies form from phase 3–4 (Figs. 10c, d, 7c, d). The height and pressure anomalies in this region can modulate the East Asian trough and the Siberian high. The above three regions are all in the path of tropospheric wave propagation (Fig. 10d).

Latitude-height cross sections of height and zonal wind anomalies over northwestern Europe are presented in Fig. 11. The negative height anomalies over the high latitudes move equatorward and downward from phase 1–3 and meanwhile their magnitude becomes larger (Fig. 11a–c). The downward propagation of positive zonal wind anomalies is also evident from phase 1 to phase 3. The downward propagation of height and zonal wind anomalies indicate the influence of stratospheric anomalies on tropospheric circulation. After the stratospheric signals reach the troposphere, the tropospheric Rossby wave train is triggered (Fig. 10b–d). After phase 4, the negative anomalies retreat to the stratosphere (Fig. 11d–f), and the tropospheric wave train weakens (Fig. 10d–f).

Downward propagation of stratospheric signal is detected over western Siberia as well. Figure 12 shows the

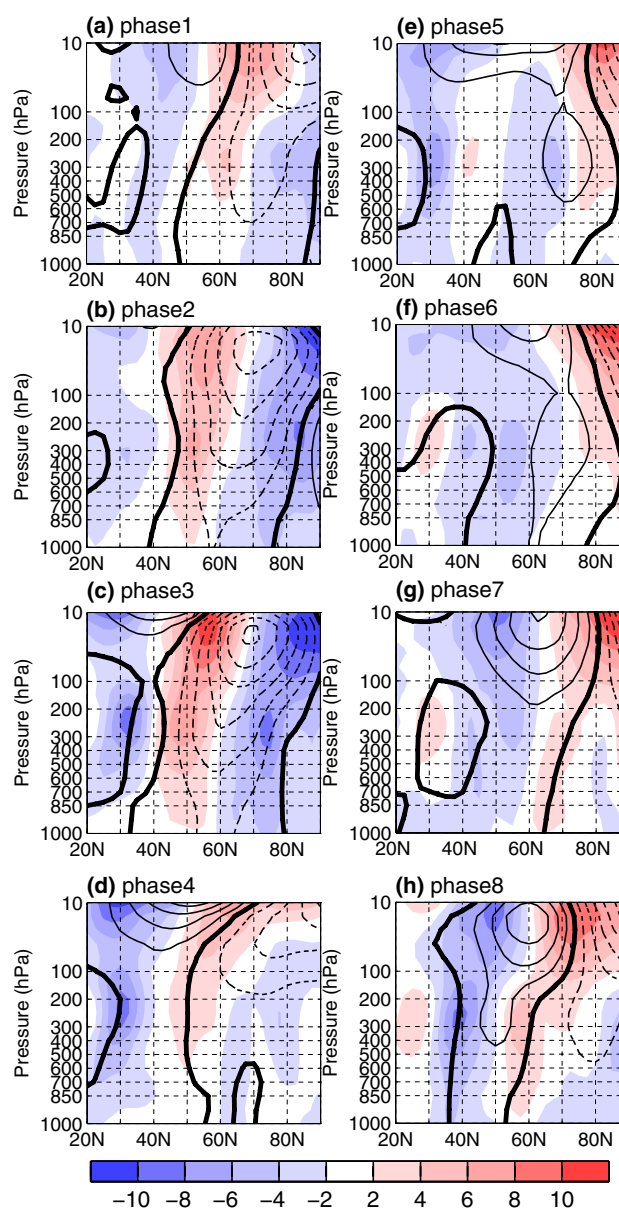


Fig. 11 Latitude-height cross section along 20°E–30°E of geopotential height anomalies (contour, interval: 40, unit: gpm) and zonal wind anomalies (shading, unit: m/s) in phases 1 to 8 of PC2 life cycle

longitude-height cross section of geopotential height and temperature anomalies along 65°N. Positive height anomalies appear in the stratosphere over northeastern Eurasia in phase 1 (Fig. 12a). The positive anomalies move westward in phase 2 (Fig. 12b), which corresponds to the clockwise rotation of the PC2 pattern. A westward tilting structure is obvious at this phase. The positive height anomalies extend downward from phase 2 to phase 3 (Fig. 12b, c), which corresponds to the increase of 300-hPa height anomalies over Siberia (Fig. 10b–d). The downward propagation of positive temperature anomalies over Siberia is evident as well

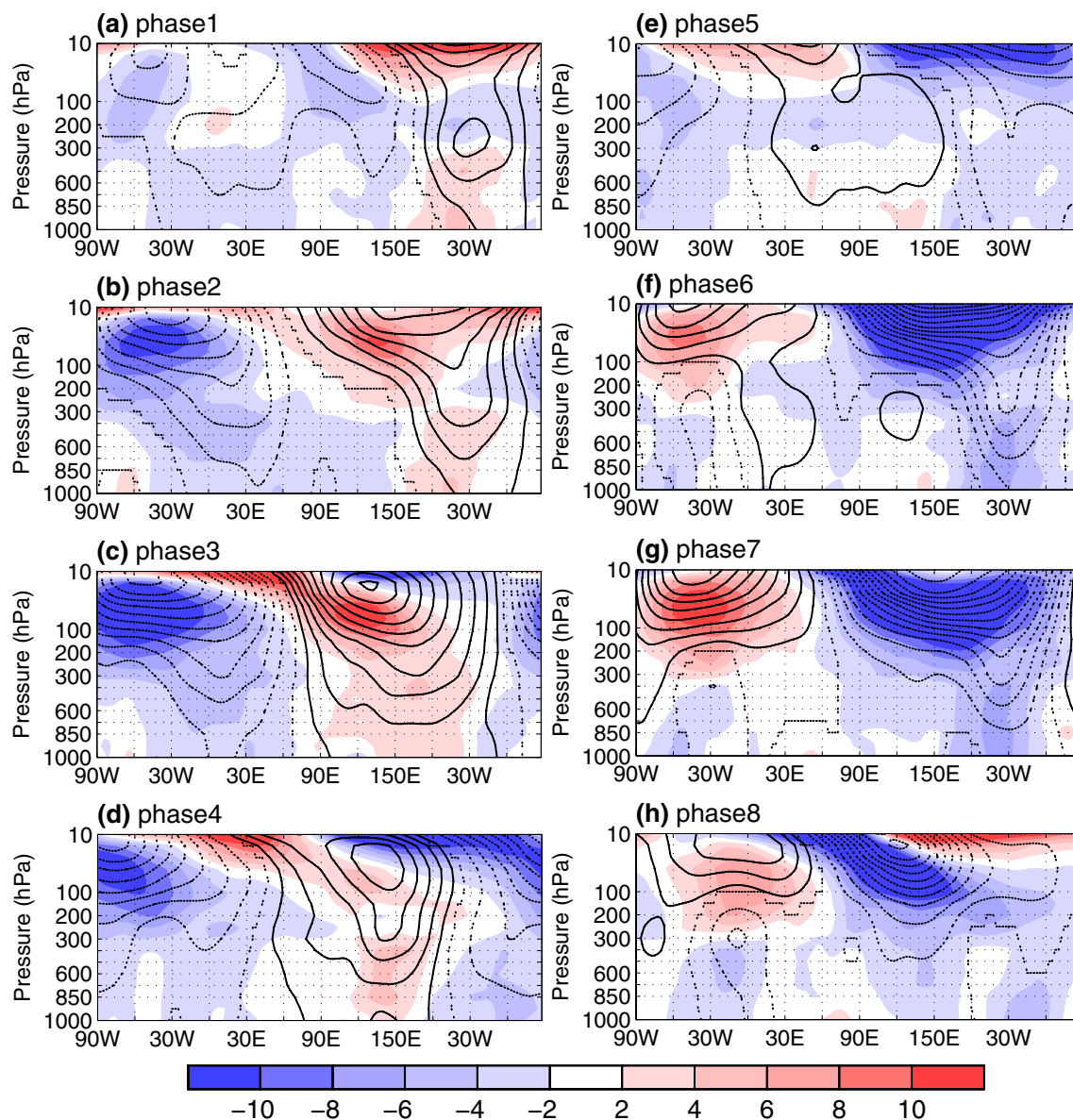


Fig. 12 Longitude-height cross section along 65°N of geopotential height anomalies (contour, interval: 40, unit: gpm) and temperature anomalies (shading, unit: °C) in phases 1–8 of PC2 life cycle

(Fig. 12b, c). This indicates a contribution of the downward propagation of stratospheric signal over Siberia. This agrees with Jeong et al. (2006) who indicated a role of the potential vorticity anomalies of the stratosphere in the increase of geopotential height over northern Eurasia. After phase 5, with the clockwise movement of the PC2 pattern, the positive height anomalies are replaced by negative anomalies (Fig. 12e–h), and the downward propagation of negative height anomalies occur from phase 6 to phase 7 (Fig. 12f, g).

Positive height anomalies in the stratosphere extend downward over the high latitudes from phase 2 to phase 5 over East Asia (Fig. 13b–d). This may contribute to the strengthening of the Siberian high (Fig. 7c, d). However,

the tropospheric negative height anomalies over eastern China in phases 3–4 have no precursory stratospheric signal (Fig. 13a–d). As such, we infer that the negative geopotential height anomalies in the troposphere over East Asia are mainly due to the downstream effect of the Rossby wave propagation over the mid-high latitudes of Eurasia. This result differs from Woo et al. (2015) who stated that the regional downward propagation of stratospheric signal contributes to the development of the East Asian trough. This difference is related to the latitudinal band in concern. Woo et al. (2015)'s analysis was based on higher latitudes (north of 50°N).

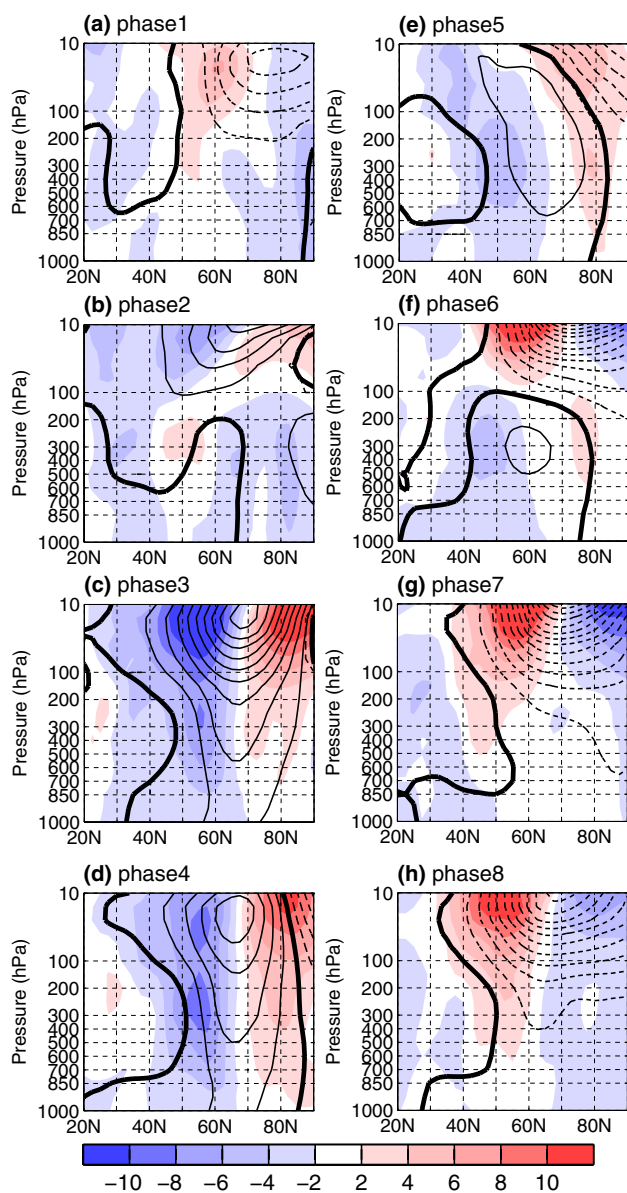


Fig. 13 The same as Fig. 11 except along 100°E–120°E

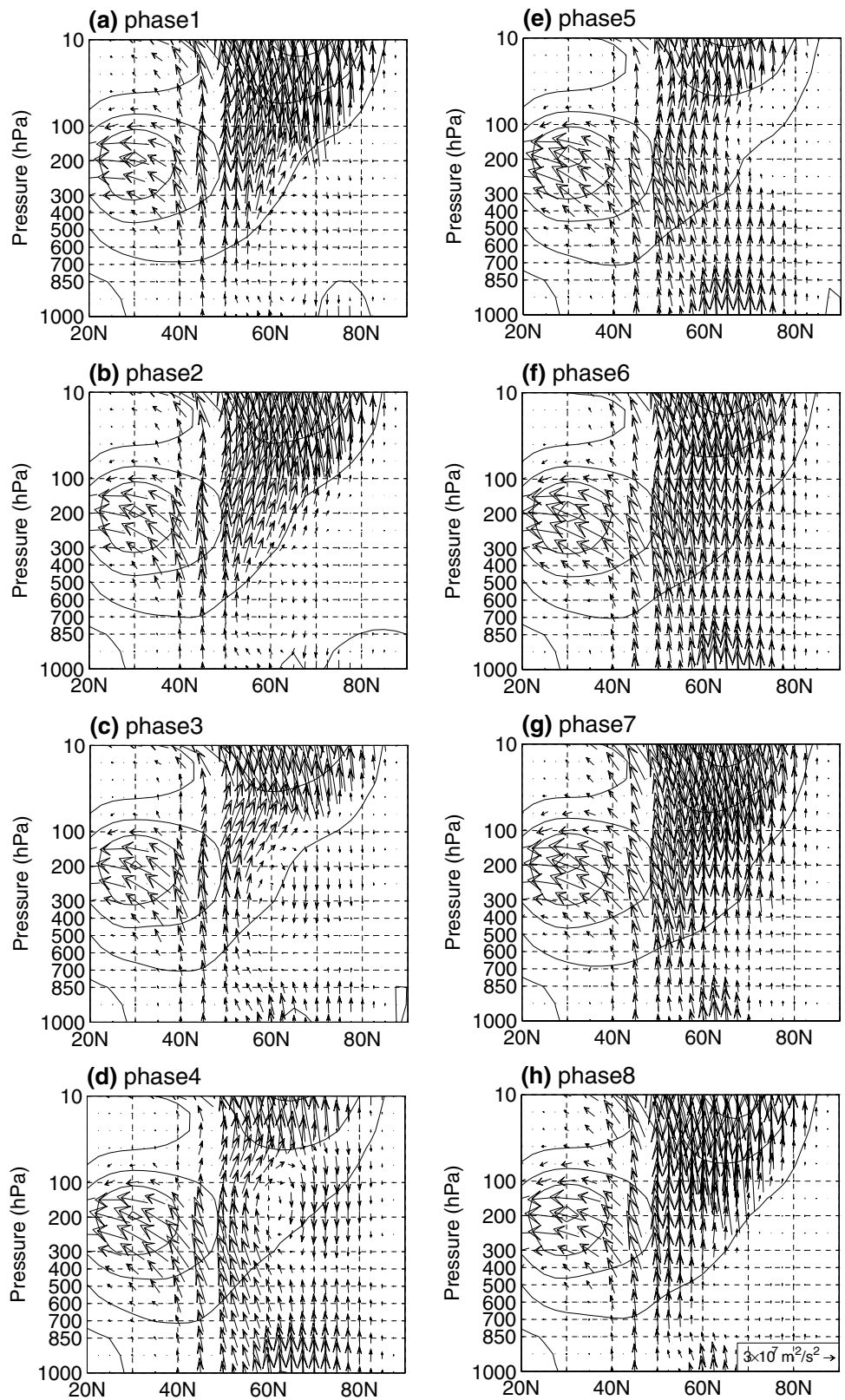
From above analysis, the stratospheric planetary wave pattern may influence the tropospheric circulation through the following pathways. One is the downward extension of stratospheric signal over western Europe during phases 1–3 of the PC2 life cycle (Fig. 11a–c), which contributes to the development of the tropospheric mid-latitude Rossby wave source (Fig. 10b–d). Another is the westward movement of stratospheric height anomalies from northeastern Eurasia to western Siberia that then descend to the troposphere during phases 1–4 of the PC2 life cycle (Fig. 12a–d). They both contribute to the building of the Rossby wave train over the mid-high latitude Eurasia. The downstream propagation of the Rossby wave train contributes to the cold events over East Asia through modulating the Siberian high and the

East Asian trough. Moreover, the downward propagation of positive height anomalies over the high-latitude East Asia also contributes to the intensification of the Siberian high in phases 2 to 4 (Fig. 13b–d).

Previous studies have indicated that the reflection of stratospheric planetary waves is involved in the stratosphere-troposphere coupling and influences tropospheric anomalies (Perlwitz and Harnik 2003; Kodera et al. 2008, 2013). To understand whether the reflection of the stratospheric planetary waves contributes to the development of the tropospheric Rossby wave source over northwestern Europe (Fig. 10c) and the descending of the anomalies from northeastern Eurasia to western Siberia during phases 1–4 of the PC2 life cycle (Fig. 12a–d), the latitude-height cross section of the EP fluxes of the planetary wavenumber 1 and zonal-mean zonal winds during the PC2 life cycle is presented in Fig. 14. Upward propagation of tropospheric planetary wavenumber 1 is observed from phase 5 to phase 8 (Fig. 14e–h). Upward EP fluxes are mainly observed above mid-troposphere in phases 1–2 (Fig. 14a, b). Downward propagation of stratospheric planetary wavenumber 1 starts after phase 2, as indicated by the downward EP fluxes that peak in phase 4 (Fig. 14b–d). A whole process of planetary wave reflection is contained in the PC2 life cycle. It takes about 6 phases from the beginning of the upward propagation to the reflection of the planetary wavenumber 1 (from phase 5 to 8, then phase 8 to phase 3). The downward propagation of stratospheric planetary wavenumber 1 from phase 2 to phase 4 (Fig. 14b–d) corresponds to the downward intrusion of the height anomalies over northwestern Europe (Fig. 11b–d) and western Siberia (Fig. 12b–d).

To confirm the regions where the downward propagation of stratospheric wavenumber 1 happens, we calculate the three-dimensional Plumb fluxes (Plumb 1985). The height-longitude cross section of Plumb fluxes and eddy geopotential heights for planetary wavenumber 1 along 65°N is shown in Fig. 15. The eddy is calculated as the departure from the zonal mean (Kodera et al. 2008). Upward propagation of tropospheric planetary wavenumber 1 is indicated by upward Plumb fluxes from phases 5–8 (Fig. 15e–h). Accordingly, the ridge and trough tilt westward with height. The upward Plumb fluxes during these phases are consistent with the upward EP fluxes along 65°N in Fig. 14e–h. After phase 8, stratospheric planetary wave propagates downward to upper troposphere and the stratospheric ridge and trough begin to tilt eastward, which suggests a downward propagation of stratospheric signals (Harnik and Lindzen 2001; Perlwitz and Harnik 2003) (Fig. 15a, b). From phases 2–4, the stratospheric trough and ridge extend downward into the mid-troposphere accompanying the downward propagation of planetary wave packets over northwestern Europe and western Siberia (Fig. 15b–d). Downward propagation of stratospheric planetary waves associated with the reflection can

Fig. 14 Latitude-height section of zonal-mean zonal winds (contour, interval: 5 m/s) and Eliassen-Palm fluxes (vector, scale on the right bottom) of the planetary wavenumber 1 in phases 1–8 of PC2 life cycle



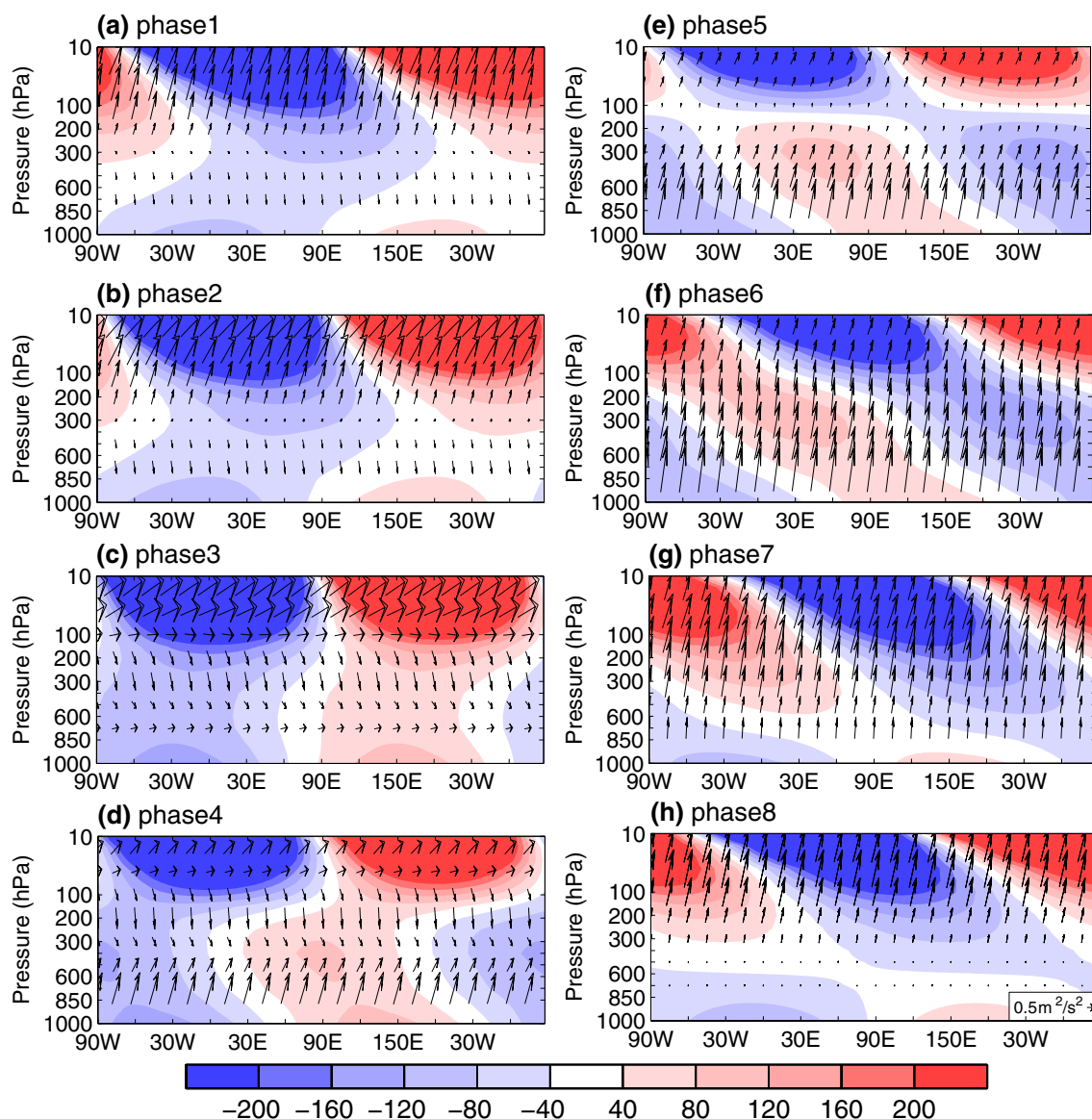


Fig. 15 Longitude-height section of eddy geopotential height (contour, unit: gpm) and Plumb fluxes (vector, scale at the right bottom) of planetary wavenumber 1 along 65°N in phases 1–8 of PC2 life cycle

amplify the tropospheric planetary waves, which provides a favorable condition for the development of tropospheric anomalies (Kodera et al. 2008, 2013, 2016). Therefore, the development of the height anomalies over northwestern Europe (Fig. 11b–d) and western Siberia (Fig. 12b–d) may be contributed by the downward propagation of stratospheric wavenumber 1.

6 Summary and discussions

Previous studies have identified a connection of tropospheric climate anomalies to the stratospheric polar vortex changes. The present study investigates the influence of the

stratospheric planetary wave pattern on cold anomalies over eastern China during November through March. The daily geopotential height variations over the high latitude stratosphere display two obvious modes that have different modulation of the stratospheric planetary wave. The two modes have about 15–20 days' time lag relationship in about 2/3 of the years. The present analysis is based on the second mode which features positive anomalies over northeastern Eurasia and negative anomalies over the North Atlantic side.

Composite analysis based on 8 phases of the temporal evolution of the stratospheric planetary wave pattern reveals clear signals in the tropospheric circulation. The geopotential height anomalies display a westward move in the troposphere, following that in the stratosphere. A Rossby wave

pattern forms over the mid-high latitudes of Eurasia in the troposphere after the peak phase of PC2. The downstream effect of the Rossby wave contributes to the deepening of the East Asian trough and southeastward expansion of the Siberian high, leading to anomalous surface northerly winds over East Asia and surface cold anomalies over eastern China.

Analysis shows that the development of the tropospheric Rossby wave train is associated with the downward propagation of stratospheric signal. Downward propagation of stratospheric signal is detected in three regions. One is western Europe which is a source region of the tropospheric Rossby wave trains. Another is western Siberia where large increase in tropospheric height anomalies is observed following the westward movement of stratospheric anomalies from north-eastern Eurasia. The third one is the high latitude East Asia where positive height anomalies propagate downward, contributing to the development of the Siberian high. Tropospheric planetary wavenumber 1 propagates upward into the stratosphere in PC2 phases 5–8 and then is reflected downward to the upper troposphere in phases 2–4, which favors the development of the height anomalies over northwestern Europe and western Siberia. In this study, we found that the deepening of the East Asian trough is not related to the downward propagation of stratospheric signal, but is mainly due to the downstream effect of the tropospheric Rossby wave train.

The results of the present study have several notable differences from previous studies. Previous studies have indicated that the weak polar vortex (i.e., planetary wavenumber 0) influences climate over East Asia. The present study reveals the impact of the stratospheric planetary wavenumber 1 pattern on the East Asian climate which have been less investigated. It is shown that the anomalies associated with the planetary wavenumber 1 pattern displays a clockwise move and the downward propagation of stratospheric anomalies is identified over western Europe, which triggers the tropospheric Rossby wave train along the polar front jet. The downward propagation of stratospheric anomalies is also detected over Siberia, which contributes to the building of the wave train. Our analysis shows that the downward stratospheric signals over both western Europe and Siberia contribute to the cold events over East Asia, whereas Jeong et al. (2006) focused on the influence of downward stratospheric signal over Siberia. Different from Woo et al. (2015), we did not find evidence of regional stratospheric-tropospheric coupling over East Asia in the deepening of the East Asian trough during the life cycle of PC2. This discrepancy may be related to the difference of the domain. The domain in our study is eastern China, whereas Woo et al. (2015) focused on the influence of weak polar vortex over the northeast part of East Asia.

The present analysis focused on the 23 of 37 years during which there is a significant positive correlation when

PC2 leads PC1. In the rest 14 years, the stratospheric polar vortex is relatively weak and the zonal-mean zonal winds in the high latitudes of the stratosphere are weaker (figure not shown). Previous studies have indicated that the strength of the stratospheric polar vortex modulates the reflection of the planetary waves (Perlwitz and Graf 2001; Perlwitz and Harnik 2003, 2004). In the rest 14 years, the weaker stratospheric polar vortex is unfavorable for the reflection of planetary waves so that PC1 and PC2 display a different lead-lag relationship. Previous studies have indicated that it may take about 12 days for the downward and upward planetary wavenumber 1 coupling between stratosphere and 500-hPa (Perlwitz and Harnik 2003, 2004). In our study, the coupling can be observed between stratosphere and lower troposphere (Fig. 14). It is expected that the upward and downward reflection in association with the lead-lag relationship between PC1 and PC2 would take more than 12 days. The composite analysis of stratospheric vacillation cycle by Kodera et al. (2013) covers a whole process of upward propagation and downward reflection of planetary waves (see their Fig. 5), which takes about 18 days. Therefore, the 15–20-day time interval between PC2 and PC1 is approximately the time for the coupling between stratospheric and lower-tropospheric planetary waves.

The present study focused on the impact of the stratospheric planetary wavenumber 1 pattern on eastern China climate. The influence of the stratospheric wave pattern upon climate in the entire North Hemisphere is worthy of study in the future. The difference of the influence of the planetary wave patterns versus that of the stratospheric polar vortex intensity change needs to be compared as well. Although the links between stratospheric circulations and tropospheric anomalies are discussed in this study, the dynamical mechanisms of how the stratospheric signal propagates downward and influences the tropospheric circulation need further investigation in the future.

Acknowledgements This study is supported by the National Natural Science Foundation of China grants (41705063, 41530425, 41475081, 41661144016, 41775080, and 41275081). The NCEP reanalysis 2 data were obtained from <ftp://ftp.cdc.noaa.gov/>.

References

- Andrews DG, Holton JR, Leovy CB (1987) Middle atmosphere dynamics. Academic Press, Cambridge
- Baldwin MP, Dunkerton TJ (1998) Biennial, quasi-biennial, and decadal oscillations of potential vorticity in the northern stratosphere. *J Geophys Res* 103:3919–3928. <https://doi.org/10.1029/97JD02150>
- Baldwin MP, Dunkerton TJ (1999) Propagation of the Arctic Oscillation from the stratosphere to the troposphere. *J Geophys Res* 104:30937–30946
- Baldwin MP, Dunkerton TJ (2001) Stratospheric harbingers of anomalous weather regimes. *Science* 294:581–584

- Baldwin MP, Stephenson DB, Thompson DWJ, Dunkerton TJ, Charlton AJ, O'Neill A (2003) Stratospheric memory and skill of extended-range weather forecasts. *Science* 301:636–640
- Bancalá S, Krüger K, Giorgetta M (2012) The preconditioning of major sudden stratospheric warmings. *J Geophys Res Atmos* 117:D04101. <https://doi.org/10.1029/2011JD016769>
- Barriopedro D, Calvo N (2014) On the relationship between ENSO, stratospheric sudden warmings, and blocking. *J Clim* 27:4704–4720
- Black RX (2002) Stratospheric forcing of surface climate in the Arctic oscillation. *J Clim* 15:268–277
- Black RX, McDaniel BA (2007) Interannual variability in the southern hemisphere circulation organized by stratospheric final warming events. *J Atmos Sci* 64:2968–2974
- Cai M, Ren R-C (2007) Meridional and downward propagation of atmospheric circulation anomalies. Part I: Northern hemisphere cold season variability. *J Atmos Sci* 64:1880–1901
- Charney JG, Drazin PG (1961) Propagation of planetary-scale disturbances from the lower into the upper atmosphere. *J Geophys Res* 66:83–109
- Chen W, Takahashi M, Graf HF (2003) Interannual variations of stationary planetary wave activity in the northern winter troposphere and stratosphere and their relations to NAM and SST. *J Geophys Res Atmos* 108:D24. <https://doi.org/10.1029/2003JD003834>
- Chen W, Yang S, Huang RH (2005) Relationship between stationary planetary wave activity and the East Asian winter monsoon. *J Geophys Res Atmos* 110:D14110. <https://doi.org/10.1029/2004JD005669>
- Coughlin K, Tung KK (2005) Tropospheric wave response to decelerated stratosphere seen as downward propagation in northern annular mode. *J Geophys Res Atmos* 110:D01103. <https://doi.org/10.1029/2004JD004661>
- Ding Y, Krishnamurti TN (1987) Heat budget of the Siberian high and the winter monsoon. *Mon Weather Rev* 115:2428–2449
- Harnik N, Lindzen RS (2001) The effect of reflecting surfaces on the vertical structure and variability of stratospheric planetary waves. *J Atmos Sci* 58:2872–2894
- Jeong J-H, Ho C-H (2005) Changes in occurrence of cold surges over East Asia in association with Arctic Oscillation. *Geophys Res Lett* 32:L14704. <https://doi.org/10.1029/2005GL023024>
- Jeong J-H, Kim B-M, Ho C-H, Chen D, Lim G-H (2006) Stratospheric origin of cold surge occurrence in East Asia. *Geophys Res Lett* 33:L14710. <https://doi.org/10.1029/2006GL026607>
- Kanamitsu M, Ebisuzaki W, Woollen J, Yang S-K, Hnilo JJ, Fiorino M, Potter GL (2002) NCEP–DOE AMIP-II reanalysis (R-2). *Bull Am Meteorol Soc* 83:1631–1643
- Kidston J, Scaife AA, Hardiman SC, Mitchell DM, Butchart N, Baldwin MP, Gray LJ (2015) Stratospheric influence on tropospheric jet streams, storm tracks and surface weather. *Nature Geosci* 8:433–440
- Kodera K, Yamazaki K, Chiba M, Shibata K (1990) Downward propagation of upper stratospheric mean zonal wind perturbation to the troposphere. *Geophys Res Lett* 17:1263–1266
- Kodera K, Kuroda Y, Pawson S (2000) Stratospheric sudden warmings and slowly propagating zonal-mean zonal wind anomalies. *J Geophys Res Atmos* 105:12351–12359
- Kodera K, Mukougawa H, Itoh S (2008) Tropospheric impact of reflected planetary waves from the stratosphere. *Geophys Res Lett* 35:L16806. <https://doi.org/10.1029/2008GL034575>
- Kodera K, Mukougawa H, Fujii A (2013) Influence of the vertical and zonal propagation of stratospheric planetary waves on tropospheric blockings. *J Geophys Res Atmos* 118:8333–8345. <https://doi.org/10.1002/jgrd.50650>
- Kodera K, Mukougawa H, Maury P, Ueda M, Claud C (2016) Absorbing and reflecting sudden stratospheric warming events and their relationship with tropospheric circulation. *J Geophys Res Atmos* 121:80–94. <https://doi.org/10.1002/2015JD023359>
- Kolstad EW, Breiteig T, Scaife AA (2010) The association between stratospheric weak polar vortex events and cold air outbreaks in the Northern Hemisphere. *Q J R Meteorol Soc* 136:886–893
- Mitchell DM, Gray LJ, Anstey J, Baldwin MP, Charlton-Perez AJ (2013) The influence of stratospheric vortex displacements and splits on surface climate. *J Clim* 26:2668–2682
- Nath D, Chen W, Zelin C, Pogoreltsev AI, Wei K (2016) Dynamics of 2013 sudden stratospheric warming event and its impact on cold weather over Eurasia: role of planetary wave reflection. *Sci Rep* 6:24174
- North GR, Bell TL, Cahalan RF, Moeng FJ (1982) Sampling errors in the estimation of empirical orthogonal functions. *Mon Weather Rev* 110:699–706
- Panagiotopoulos F, Shahgedanova M, Hannachi A, Stephenson DB (2005) Observed trends and teleconnections of the Siberian high: a recently declining center of action. *J Clim* 18:1411–1422
- Perlwitz J, Graf H-F (2001) Troposphere-stratosphere dynamic coupling under strong and weak polar vortex conditions. *Geophys Res Lett* 28:271–274
- Perlwitz J, Harnik N (2003) Observational evidence of a stratospheric influence on the troposphere by planetary wave reflection. *J Clim* 16:3011–3026
- Perlwitz J, Harnik N (2004) Downward coupling between the stratosphere and troposphere: the relative roles of wave and zonal mean processes. *J Clim* 17:4902–4909
- Plumb RA (1985) On the three-dimensional propagation of stationary waves. *J Atmos Sci* 42:217–229
- Ren RC, Cai M (2007) Meridional and vertical out-of-phase relationships of temperature anomalies associated with the Northern Annular Mode variability. *Geophys Res Lett* 34:L07704. <https://doi.org/10.1029/2006GL028729>
- Scaife AA, James IN (2000) Response of the stratosphere to interannual variability of tropospheric planetary waves. *Q J R Meteorol Soc* 126:275–297
- Scaife AA, Knight JR, Vallis GK, Folland CK (2005) A stratospheric influence on the winter NAO and North Atlantic surface climate. *Geophys Res Lett* 32:1–5. <https://doi.org/10.1029/2005GL023226>
- Scaife AA, Folland CK, Alexander LV, Moberg A, Knight JR (2008) European climate extremes and the North Atlantic Oscillation. *J Clim* 21:72–83
- Song L, Wu R (2017) Process for occurrence of strong cold events over Eastern China. *J Clim* 30:9247–9266
- Song L, Wang L, Chen W, Zhang Y (2016) Intraseasonal variation of the strength of the East Asian trough and its climatic impacts in boreal winter. *J Clim* 29:2557–2577
- Song L, Wu R, Jiao Y (2018) Relative contributions of synoptic and intraseasonal variations to strong cold events over eastern China. *Clim Dyn* 50:4619–4634
- Takaya K, Nakamura H (1997) A formulation of a wave—activity flux for stationary Rossby waves on a zonally varying basic flow. *Geophys Res Lett* 24:2985–2988
- Takaya K, Nakamura H (2001) A formulation of a phase-independent wave-activity flux for stationary and migratory quasigeostrophic eddies on a zonally varying basic flow. *J Atmos Sci* 58:608–627
- Takaya K, Nakamura H (2013) Interannual variability of the East Asian winter monsoon and related modulations of the planetary waves. *J Clim* 26:9445–9461
- Thompson DWJ, Wallace JM (1998) The Arctic Oscillation signature in the wintertime geopotential height and temperature fields. *Geophys Res Lett* 25:1297–1300
- Thompson DWJ, Baldwin MP, Wallace JM (2002) Stratospheric connection to Northern Hemisphere wintertime weather: implications for prediction. *J Clim* 15: 1421–1428

- Tomassini L, Gerber EP, Baldwin MP, Bunzel F, Giorgetta M (2012) The role of stratosphere-troposphere coupling in the occurrence of extreme winter cold spells over northern Europe. *J Adv Model Earth Syst* 4:M00A03. <https://doi.org/10.1029/2012MS000177>
- Wang L, Chen W (2010) Downward Arctic Oscillation signal associated with moderate weak stratospheric polar vortex and the cold December 2009. *Geophys Res Lett* 37:L09707. <https://doi.org/10.1029/2010GL042659>
- Wang L, Huang R, Gu L, Chen W, Kang L (2009) Interdecadal variations of the East Asian winter monsoon and their association with quasi-stationary planetary wave activity. *J Clim* 22:4860–4872
- Watanabe M (2004) Asian jet waveguide and a downstream extension of the North Atlantic Oscillation. *J Clim* 17:4674–4691
- Woo S-H, Kim B-M, Kug J-S (2015) Temperature variation over East Asia during the lifecycle of weak stratospheric polar vortex. *J Clim* 28:5857–5872
- Woollings T, Charlton-Perez A, Ineson S, Marshall AG, Masato G (2010) Associations between stratospheric variability and tropospheric blocking. *J Geophys Res Atmos* 115:06108. <https://doi.org/10.1029/2009JD012742>
- Yu Y-Y, Cai M, Ren R-C, Rao J (2018) A closer look at the relationships between meridional mass circulation pulses in the stratosphere and cold air outbreak patterns in northern hemispheric winter. *Clim Dyn*. <https://doi.org/10.1007/s00382-018-4069-7>
- Zhang Y, Sperber KR, Boyle JS (1997) Climatology and interannual variation of the East Asian winter monsoon: results from the 1979–95 NCEP/NCAR reanalysis. *Mon Weather Rev* 125:2605–2619